Stimulated-emission cross-sections of trivalent erbium ions in the cubic sesquioxides Y2O3 , Lu2O3, and Sc2O3

Anastasia Uvarova, Pavel Loiko, Sascha Kalusniak, Elena Dunina, Liudmila Fomicheva, Alexey Kornienko, Stanislav Balabanov, Alain Braud, Patrice Camy, Christian Kränkel

Stimulated-emission cross-sections of trivalent erbium ions in the cubic sesquioxides Y_2O_3, Lu_2O_3, and Sc_2O_3

Anastasia Uvarova[1], Pavel Loiko [2], Sascha Kalusniak[1], Elena Dunina[3], Liudmila Fomicheva[4], Alexey Kornienko[3], Stanislav Balabanov[5], Alain Braud[2], Patrice Camy[2], and Christian Kränkel[1,*]

[1]Leibniz-Institut für Kristallzüchtung (IKZ), Max-Born-Str. 2, 12489 Berlin, Germany
[2]Centre de Recherche sur les Ions, les Matériaux et la Photonique (CIMAP), UMR 6252 CEA-CNRS-ENSICAEN, Université de Caen, 6 Boulevard Maréchal Juin, 14050 Caen Cedex 4, France
[3]Vitebsk State Technological University, 72 Moskovskaya Ave., 210035 Vitebsk, Belarus
[4]Belarusian State University of Informatics and Radioelectronics, 6 Brovka St., 220027, Minsk, Belarus
[5]G. G. Devyatykh Institute of Chemistry of High-Purity Substances of RAS, 49 Tropinin St., 603951 Nizhny Novgorod, Russia
**christian.kraenkel@ikz-berlin.de*

Abstract: We report on a detailed revision of the spectroscopic properties of Er^{3+} ions in the cubic sesquioxide host crystals R_2O_3 (R = Y, Lu and Sc). The 4f-4f transition probabilities are calculated by applying a modified Judd-Ofelt theory accounting for configuration interaction based on the measured absorption spectra. The stimulated-emission cross-sections for the $^4I_{11/2} \rightarrow {}^4I_{13/2}$ (at ~2.8 μm) and $^4I_{13/2} \rightarrow {}^4I_{15/2}$ (at ~1.6 μm) transitions of Er^{3+} ions are determined and the luminescence dynamics from the $^4I_{11/2}$ and $^4I_{13/2}$ manifolds are studied at different temperatures. It is found that the luminescence lifetime of the $^4I_{11/2}$ state strongly depends on the host-forming R^{3+} cation even at low temperatures due to a non-negligible non-radiative multiphonon decay channel. Er:Y_2O_3 exhibits the lowest phonon energies and consequently the longest $^4I_{11/2}$ luminescence lifetimes. A disagreement between the absorption and emission probabilities for the $^4I_{15/2} \leftrightarrow {}^4I_{11/2}$ transition of Er^{3+} ions is observed at room temperature and explained considering the distribution of Er^{3+} ions over two non-equivalent crystallographic sites, C_2 and C_{3i}.

1. Introduction

Trivalent erbium ions (Er^{3+}) possess the electronic configuration [Xe]$4f^{11}$ with the ground-state $^4I_{15/2}$. They feature a complex and dense energy level scheme allowing for multiple emission lines in the visible, near and mid-infrared spectral ranges, as well as efficient energy-transfer processes. As shown in Fig. 1, the two most commonly exploited laser transitions of Er^{3+} ions are the transitions $^4I_{13/2} \rightarrow {}^4I_{15/2}$ at wavelengths around 1.55 μm and $^4I_{11/2} \rightarrow {}^4I_{13/2}$ at wavelengths around 2.85 μm. In particular the latter attracts attention for medical applications, driving sources for nonlinear processes or trace gas analysis in the molecular fingerprint region [1-3].

Among the host materials suitable for Er^{3+} doping with the goal of achieving laser emission in the 3 μm range, the rare-earth sesquioxides R_2O_3, where R stands for the host cations Y, Lu or Sc attracted a lot of attention [4]. These compounds crystallize in the cubic space group $Ia\bar{3}$ adopting the body-centered bixbyite structure. Cubic sesquioxide crystals feature attractive thermo-physical properties such as a high thermal conductivity of more than 12 $Wm^{-1}K^{-1}$ for undoped Lu_2O_3 at room temperature, a weak thermal expansion coefficient as well as small and positive thermo-optic coefficients [5]. Moreover, their maximum phonon energies below 700 cm^{-1} [6] are moderate for oxide materials leading to reduced non-radiative multiphonon relaxation [7] in particular for transitions from the $^4I_{11/2}$ manifold. Finally, they exhibit strong

crystal-fields for the dopant Er^{3+} ions leading to broad emission spectra. Isostructural substitutional solid-solutions are formed in the $R_2O_3 – Er_2O_3$ binary systems allowing for the formation of cubic sesquioxides even at Er^{3+} high doping levels. The latter is relevant for the development of 2.8 µm lasers as high Er^{3+} doping concentrations strongly increase the probability for energy-transfer upconversion from the metastable terminal laser level $^4I_{13/2}$, avoiding high population of this level which may otherwise lead to self-termination of lasers based on the $^4I_{11/2} \rightarrow {}^4I_{13/2}$ transition [8].

Note that cubic sesquioxides in general and Er^{3+}-doped compounds in particular can be obtained in the form of transparent polycrystalline ceramics benefiting from lower synthesis temperatures of around 1800 °C as compared to sesquioxide single-crystals with melting points in excess of 2400 °C [9, 10].

Highly-efficient and power-scalable crystalline and ceramic Er^{3+}-doped sesquioxide lasers operating on the $^4I_{11/2} \rightarrow {}^4I_{13/2}$ transition are known. Li *et al*. reported on a crystalline Er:Lu_2O_3 laser pumped by an optically pumped semiconductor laser delivering 1.4 W at 2.85 µm with a slope efficiency as high as 36%. Under diode-pumping, the output was scaled up to 5.9 W at the expense of a reduced slope efficiency of 27% [11]. Yao *et al*. developed a diode-pumped Er:Lu_2O_3 ceramic laser generating 6.7 W at 2.85 µm with a slope efficiency of 30.2% [9] and more recently, a diode-pumped Er:Y_2O_3 ceramic laser enabled an output power of 13.4 W at 2.7 µm at room temperature [12]. By operation at cryogenic temperatures, even higher output power levels are feasible at 2.85 µm [13].

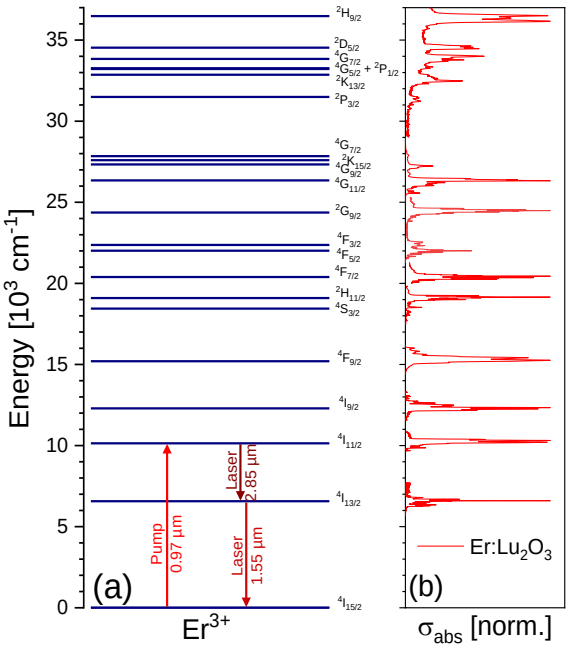

Fig. 1. (a) Energy level scheme [14] of Er^{3+} ions showing laser transitions at 1.6 µm and 2.8 µm and the energy levels relevant for the absorption measurements and calculations within this work. (b) Absorption cross sections normalized for the highest peak in the respective range indicating that all expected energy levels were detected in the absorption measurements.

Despite their wide use in lasers, the spectroscopic properties of Er^{3+}-doped sesquioxides, and, in particular, the transition probabilities at 2.85 µm, remain not completely understood. There are two common methods to calculate the stimulated-emission cross-sections for rare-earth ions. The Füchtbauer-Ladenburg equation [15] relies on the directly measured luminescence spectrum and the radiative lifetime τ_{rad} of the emitting level. In cases where more

than one terminal level for the emission exists, the luminescence branching ratio B(JJ') for each transition J → J' needs to be determined. τ_{rad} and B(JJ') are often obtained using theoretical calculations for f-f transition intensities known as Judd-Ofelt theory [16, 17]. Another approach relies on the reciprocity method (RM) known as McCumber equation [18, 19], using Einstein's theory of equal transition probabilities for absorption and emission between two Stark levels [20].

One of the main challenges for determining the spectroscopic properties of rare-earth ions in cubic sesquioxides is a disagreement between the experimental absorption and emission probabilities for certain optical transitions. It was suggested that such a disagreement may originate from different oscillator strengths for rare-earth ions incorporated on two non-equivalent sites in the cubic bixbyite structure [21], having the symmetries C_2 and C_{3i} (Wyckoff: 24*d* and 8*b*, respectively) and a sixfold oxygen coordination. The unit-cell of cubic sesquioxide crystals contains 32 cation sites and for an ideal structure, 3/4 of the cations occupy C_2 sites and 1/4 occupies C_{3i} sites. This proportion is expected to hold also for rare-earth doping ions. Theoretical models suggest a deviation from this behavior at room-temperature for Er:Sc_2O_3 [22], but these models are not valid at the high growth temperatures of this material and due to the low mobility of cations at room temperature, the random distribution at high temperatures can be expected to be maintained at room temperature. Due to the presence of a center of inversion, electric dipole (ED) transitions are forbidden for rare-earth ions residing on C_{3i} sites. Still, these ions can contribute to transition intensities with a magnetic dipole (MD) component, *i.e.*, J ↔ J' transitions with ΔJ = 0, ±1 (except for 0 ↔ 0'). Note that both the $^4I_{11/2}$ ↔ $^4I_{13/2}$ as well as the $^4I_{13/2}$ ↔ $^4I_{15/2}$ transition are ED and MD allowed while the transition $^4I_{11/2}$ ↔ $^4I_{15/2}$ is MD forbidden due to ΔJ = 2.

To determine the stimulated-emission cross-sections of Er^{3+} ions in cubic sesquioxides, we performed a comparative study of the absorption and emission probabilities for the three cubic sesquioxides yttria (Y_2O_3), lutetia (Lu_2O_3) and scandia (Sc_2O_3). This study involved the Judd-Ofelt analysis, the measurement of the absorption and emission spectra, as well as the luminescence dynamics as a function of temperature. Even though the three studied compounds are isostructural, they exhibit significantly different properties in terms of the lattice parameter and phonon energies, which is explained by the different sizes and masses of the host-forming cations. This also leads to a strong variation of the spectroscopic parameters within this host crystal family.

2. Absorption spectra and Judd-Ofelt analysis

Figure 2 shows the absorption cross-section spectra for Er^{3+} ions in Y_2O_3, Lu_2O_3 and Sc_2O_3 crystals. For the $^4I_{15/2}$ → $^4I_{11/2}$ transition which is commonly used for pumping of mid-infrared Er^{3+} lasers, the peak absorption cross sections amount to 0.35×10^{-20} cm^2 at 974.2 nm, 0.30×10^{-20} cm^2 at 980.7 nm, and 0.33×10^{-20} cm^2 at 979.3 nm, respectively.

Based on these data, the transition intensities of Er^{3+} ions in the three sesquioxide crystals were determined using the Judd-Ofelt formalism [16, 17]. The experimental absorption oscillator strengths f_{exp} were calculated as:

$$f_{exp}(\mathrm{JJ'}) = \frac{m_e c^2}{\pi e^2 \langle\lambda\rangle^2} \Gamma(\mathrm{JJ'}), \tag{1}$$

where m_e and e are the electron mass and charge, respectively, c is the speed of light, Γ(JJ') is the integrated absorption cross-section within the absorption band for the J → J' transition, and $\langle\lambda\rangle$ is the wavelength corresponding to the barycenter of the absorption band. The experimental absorption oscillator strengths f_{exp} and the values f_{calc} calculated by three different approaches detailed below are given in Table 1 for the example of Er:Lu_2O_3.

Table 1. Experimental and calculated absorption oscillator strengths for Er^{3+} ions in Lu_2O_3

$^4I_{15/2} \rightarrow {}^{2S+1}L_J$	E_J, cm^{-1}	Γ, 10^{-20} $cm^{-2}nm$	f_{exp}, 10^{-6} (ED + MD)	f_{calc}, 10^{-6} J-O	mJ-O	ICI
$^4I_{13/2}$	6600	30.81	1.516	0.931^{ED} + 0.599^{MD}	0.984^{ED} + 0.599^{MD}	0.846^{ED} + 0.599^{MD}
$^4I_{11/2}$	10196	3.708	0.437	0.511^{ED}	0.527^{ED}	0.499^{ED}
$^4I_{9/2}$	12466	1.720	0.300	0.156^{ED}	0.242^{ED}	0.229^{ED}
$^4F_{9/2}$	15222	5.861	1.538	1.286^{ED}	1.574^{ED}	1.567^{ED}
$^4S_{3/2} + {}^2H_{11/2}$	18978	23.83	9.799	9.030^{ED}	9.769^{ED}	9.798^{ED}
$^4F_{7/2}$	20303	2.742	1.281	1.338^{ED}	1.248^{ED}	1.336^{ED}
$^4F_{5/2} + {}^4F_{3/2}$	22116	0.774	0.428	0.676^{ED}	0.545^{ED}	0.581^{ED}
$^2G_{9/2}$	24404	1.199	0.811	0.528^{ED}	0.441^{ED}	0.504^{ED}
$^4G_{11/2} + {}^2K_{15/2}$ + $^4G_{9/2} + {}^2G_{7/2}$	26561	24.81	19.58	19.87^{ED} + 0.070^{MD}	19.52^{ED} + 0.070^{MD}	19.50^{ED} + 0.070^{MD}
r.m.s. dev.				0.369	0.168	0.184

E_J – experimental barycenter energy of the multiplet, Γ – integrated absorption cross-section, f_{exp} and f_{calc} – experimental and calculated absorption oscillator strengths, respectively, ED – electric-dipole, MD – magnetic-dipole, r.m.s. dev. – root mean square deviation between f_{exp} and f_{calc}.

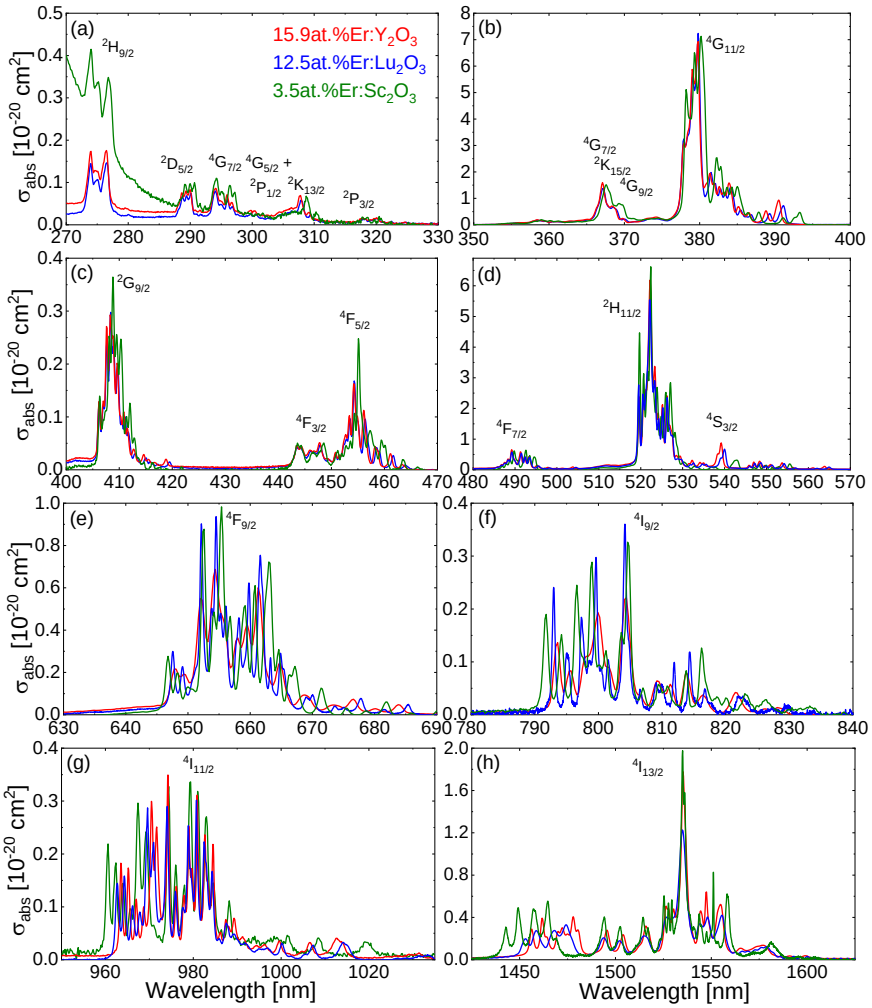

Fig. 2. (a-h) Ground-state absorption cross-sections σ_{abs} of Er^{3+} ions in Y_2O_3, Lu_2O_3 and Sc_2O_3 crystals for the energy levels shown in Fig. 1. The UV absorption background for Er:Sc_2O_3 in (a) is attributed to color centers and was subtracted for the J-O-calculations.

The electric dipole (ED) contribution to the calculated absorption oscillator strengths f_{calc} of a transition can be determined from the corresponding line strengths S(JJ'):

$$f_{calc}^{ED}(JJ') = \frac{8}{3h(2J'+1)\langle\lambda\rangle}\frac{\left(\langle n\rangle^2+2\right)^2}{9n}S_{calc}^{ED}(JJ'), \quad (2)$$

where h is the Planck constant and n is the refractive index calculated from the dispersion formulas for cubic sesquioxide crystals given in [23].

Three different models were applied to calculate the ED contributions to the line strengths of f-f transitions of Er^{3+} ions, (i) the standard Judd-Ofelt (J-O) theory and two modifications accounting for configuration interaction, (ii) the modified Judd-Ofelt theory (mJ-O) and (iii) the approximation of an intermediate configuration interaction (ICI) [24, 25]. The contributions of magnetic-dipole (MD) transitions were calculated independently within the Russell-Saunders approximation on wave functions of Er^{3+} under the assumption of a free-ion.

For the standard J-O theory, the ED line strengths for a transition J → J' are:

$$S_{calc}^{ED}(JJ') = \sum_{k=2,4,6} U^{(k)}\Omega_k, \quad (3a)$$

$$U^{(k)} = \langle (4f^n)SLJ \| U^k \| (4f^n)S'L'J' \rangle^2 . \quad (3b)$$

Here, $U^{(k)}$ (k = 2, 4, 6) are the reduced squared matrix elements calculated using the free-ion parameters reported in [26], and Ω_k are the three intensity (J–O) parameters.

In the ICI approximation, the ED line strengths become

$$S_{calc}^{ED}(JJ') = \sum_{k=2,4,6} U^{(k)}\tilde{\Omega}_k, \quad (4a)$$

$$\tilde{\Omega}_k = \Omega_k[1+2R_k(E_J + E_{J'} - 2E_f^0)], \quad (4b)$$

where the intensity parameters $\tilde{\Omega}_k$ depend linearly on the energies E_J and $E_{J'}$ of the two multiplets involved in the transition, E_f^0 has the meaning of the average energy of the $4f^{11}$ Er^{3+} configuration, and R_k (k = 2, 4, 6) are the parameters representing the configuration interaction. Consequently, there are six free parameters, namely Ω_k and R_k for k = 2, 4, and 6, each.

Assuming that only the excited configuration with opposite parity $4f^{10}5d^1$ contributes to the configuration interaction, $R_2 = R_4 = R_6 = \alpha \approx 1/(2\Delta)$ and Eq. (4b) is simplified to

$$\tilde{\Omega}_k = \Omega_k[1+2\alpha(E_J + E_{J'} - 2E_f^0)]. \quad (5)$$

This approximation is referred to as the modified J-O (mJ-O) theory and it corresponds to only four free parameters, namely Ω_2, Ω_4, Ω_6 and α. In this model, Δ is the energy of the excited configuration $4f^{10}5d^1$ of Er^{3+}. It should be noted that for high $4f^{10}5d^1$ energies ($\Delta \to \infty$, $\alpha \to 0$), Eq. (5) yields the formula for the standard J-O model.

The absorption oscillator strengths for Er^{3+} ions in sesquioxides were calculated using all three above-mentioned models. The root mean square (r.m.s.) deviation between f_{exp} and f_{calc} (ED + MD) values was determined, as shown in Table 1 for the case of Er:Lu_2O_3. The ICI model provides the lowest r.m.s. deviation and the best agreement between the experimental and calculated transition intensities for the $^4I_{13/2}$ and $^4I_{11/2}$ excited states. Thus, it was selected for further calculations.

The resulting intensity parameters of the standard J-O and ICI models for Er^{3+} ions for the three host materials under investigation here are listed in Table 2.

Table 2. Intensity parameters for Er^{3+} ions in cubic sesquioxide host materials (J-O and ICI models)

Parameter	Y_2O_3		Lu_2O_3		Sc_2O_3	
	J-O	ICI	J-O	ICI	J-O	ICI
Ω_2, 10^{-20} cm^2	4.520	4.478	4.933	5.115	4.626	4.309
Ω_4, 10^{-20} cm^2	1.313	1.511	0.635	1.042	2.306	1.721
Ω_6, 10^{-20} cm^2	0.511	0.479	0.667	0.570	0.516	0.671
R_2, 10^{-4} cm		-0.048		-0.106		0.182
R_4, 10^{-4} cm		0.092		0.061		-0.035
R_6, 10^{-4} cm		0.002		0.011		0.020

The probabilities of spontaneous radiative transitions (ED + MD) were calculated from the corresponding line strengths:

$$A_{\Sigma}^{calc}(JJ') = \frac{64\pi^4 e^2}{3h(2J'+1)\langle\lambda\rangle^3} n\left(\frac{n^2+2}{3}\right)^2 S_{ED}^{calc}(JJ') + A_{MD}(JJ'). \quad (6)$$

The A_{MD}(JJ') contributions are calculated separately as explained above for the transitions in absorption. Then, the radiative lifetimes of the excited states τ_{rad} and the luminescence branching ratios for the particular emission channels B(JJ') were derived:

$$\tau_{rad} = \frac{1}{A_{tot}^{calc}}, \text{ where } A_{tot}^{calc} = \sum_{J'} A_{\Sigma}^{calc}(JJ'), \text{ and } B(JJ') = \frac{A_{\Sigma}^{calc}(JJ')}{\sum_{J'} A_{\Sigma}^{calc}(JJ')}. \quad (7)$$

The results on the transition probabilities in emission for Er^{3+}:Lu_2O_3 are shown in Table 3.

Table 3. Probabilities of spontaneous radiative transitions of Er^{3+} ions in Lu_2O_3 (ICI model)

Emitting state	Terminal state	$\langle\lambda_{em}\rangle$, nm	A(JJ'), s^{-1}	B(JJ')	A_{tot}, s^{-1}	τ_{rad}, ms
$^4I_{13/2}\rightarrow$	$^4I_{15/2}$	1515	$101.98^{ED} + 72.15^{MD}$	1	174.1	5.74
$^4I_{11/2}\rightarrow$	$^4I_{13/2}$	2781	$18.41^{ED} + 15.19^{MD}$	0.167	201.5	4.96
	$^4I_{15/2}$	980.8	167.86^{ED}	0.833		
$^4I_{9/2}\rightarrow$	$^4I_{11/2}$	4405	$1.00^{ED} + 2.42^{MD}$	0.019	182.9	5.47
	$^4I_{13/2}$	1705	39.16^{ED}	0.214		
	$^4I_{15/2}$	802.2	140.28^{ED}	0.767		
$^4F_{9/2}\rightarrow$	$^4I_{9/2}$	3628	$5.32^{ED} + 4.24^{MD}$	0.006	1613	0.619
	$^4I_{11/2}$	1990	$63.85^{ED} + 10.44^{MD}$	0.046		
	$^4I_{13/2}$	1160	81.51^{ED}	0.050		
	$^4I_{15/2}$	656.9	1447.83^{ED}	0.898		
$^4S_{3/2} + {}^2H_{11/2}\rightarrow$	$^4F_{9/2}$	2662	$28.72^{ED} + 0.26^{MD}$	0.002	13407	0.075
	$^4I_{9/2}$	1536	$165.99^{ED} + 1.13^{MD}$	0.012		
	$^4I_{11/2}$	1139	$117.13^{ED} + 14.11^{MD}$	0.011		
	$^4I_{13/2}$	807.9	$544.87^{ED} + 117.77^{MD}$	0.049		
	$^4I_{15/2}$	526.9	12417.1^{ED}	0.926		
$^4F_{7/2}\rightarrow$	$^4S_{3/2} + {}^2H_{11/2}$	7547	0.91^{ED}	0.000	3817	0.262
	$^4F_{9/2}$	1968	$7.53^{ED} + 19.60^{MD}$	0.007		
	$^4I_{9/2}$	1276	$122.24^{ED} + 17.94^{MD}$	0.037		
	$^4I_{11/2}$	989.4	258.44^{ED}	0.068		
	$^4I_{13/2}$	729.8	621.27^{ED}	0.163		
	$^4I_{15/2}$	492.5	2769.2^{ED}	0.725		

$\langle\lambda_{em}\rangle$ – mean emission wavelength, ED – electric-dipole, MD – magnetic-dipole, A(JJ') – probability of spontaneous radiative transition, B(JJ') – luminescence branching ratio, τ_{rad} – radiative lifetime of an excited state. The $^4S_{3/2} + {}^2H_{11/2}$ levels are considered as thermally coupled.

Table 4 summarizes the radiative lifetimes of the $^4I_{13/2}$ and $^4I_{11/2}$ excited states and the luminescence branching ratios B(JJ') for the $^4I_{11/2} \rightarrow {}^4I_{13/2}$ transition for all three studied sesquioxides. These values are relevant for further calculations of the stimulated-emission cross-sections for the $^4I_{11/2} \rightarrow {}^4I_{13/2}$ and $^4I_{13/2} \rightarrow {}^4I_{15/2}$ transitions of Er^{3+} ions in these hosts as well as the interpretation of the results of the measurements of the luminescence dynamics.

Table 4. Selected radiative lifetimes and luminescence branching ratios for Er^{3+} ions in cubic sesquioxide crystals (ICI model)

Crystal	$^4I_{13/2}$ τ_{rad}, ms	$^4I_{11/2}$ τ_{rad}, ms	$^4I_{11/2} \rightarrow {}^4I_{13/2}$ $B(JJ')$, %	$^4I_{13/2}$ (MD) τ_{rad}, ms
Er:Y_2O_3	5.79	5.39	18.3	13.22
Er:Lu_2O_3	5.74	4.96	16.7	13.86
Er:Sc_2O_3	5.64	5.57	21.2	14.73

3. Experimental verification of the results of the Judd-Ofelt analysis

One possibility to estimate the ratio of $B(JJ')$ and τ_{rad} by experimental methods, is to simultaneously use two independent methods for calculating the stimulated-emission cross-sections σ_{SE}, namely the Füchtbauer-Ladenburg (F-L) equation [15] and the reciprocity method (RM). This approach can be applied to any transition occurring between the ground-state and an excited-state, but for the particular case of sesquioxides, the presence of doping ions on the two sites C_2 and C_{3i} may lead to wrong results. However, as explained above, for ions on C_{3i} sites, only MD transitions are allowed. The MD-forbidden $^4I_{11/2} \rightarrow {}^4I_{15/2}$ transition leading to emission around 1 μm is thus a good candidate to widely exclude the influence of ions on C_{3i} sites. The Füchtbauer-Ladenburg equation is:

$$\sigma_{SE}(\lambda) = \frac{\lambda^5}{8\pi < n >^2 \tau_{rad} c} \frac{B(JJ')W'(\lambda)}{\int \lambda W'(\lambda) d\lambda}, \quad (8)$$

where, λ is the light wavelength, $<n>$ is the refractive index at the mean emission wavelength $<\lambda_{em}>$, τ_{rad} is the radiative lifetime of the emitting state, $B(JJ')$ is the luminescence branching ratio for the considered transition, and $W'(\lambda)$ is the luminescence spectrum corrected for the apparatus function of the set-up.

The SE cross-sections are calculated via the reciprocity method as:

$$\sigma_{SE}(\lambda) = \sigma_{abs}(\lambda) \frac{Z_1}{Z_2} \exp\left(-\frac{(hc/\lambda) - E_{ZPL}}{kT} \right), \quad (9a)$$

$$Z_m = \sum_k g_k^m \exp(-E_k^m / kT). \quad (9b)$$

Here, k is the Boltzmann constant, T is the temperature, E_{ZPL} is the energy of the zero-phonon-line (ZPL) transition between the lowest Stark sub-levels of the involved multiplets (10192 cm^{-1} [27]), Z_m are the partition functions of the lower (m = 1) and upper (m = 2) manifold (Z_1/Z_2 = 1.046 [27]), and g_k^m is the degeneracy of the Stark sub-level k and energy E_k^m relative to the lowest sub-level of each multiplet.

By comparing Eq. (8) and (9a), one can estimate $B(JJ')/\tau_{rad}$. Such an analysis was performed for the $^4I_{11/2} \rightarrow {}^4I_{15/2}$ transition of Er^{3+} ions in Lu_2O_3, as shown in Fig. 3. Note that in the spectral range of strong overlap between absorption and emission, the luminescence intensity can decrease owing to reabsorption. This was widely avoided by applying the pinhole-method for the luminescence measurements [28-30]. For photon energies well above the ZPL energy, the reciprocity method yields strong noise due to the exponential term in Eq. (9a). The best matching between the areas under the σ_{SE} curves obtained using both methods was achieved for $B(JJ')/\tau_{rad} = 155 \pm 5\ s^{-1}$.

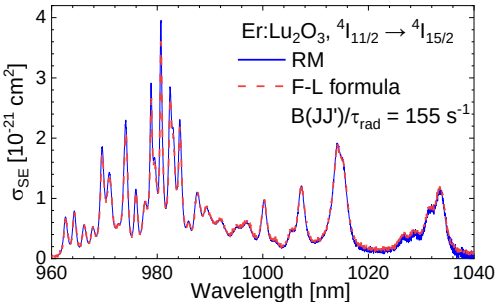

Fig. 3. Comparison of the stimulated-emission cross-sections σ_{SE}, for the $^4I_{11/2} \rightarrow {}^4I_{15/2}$ transition of Er^{3+} ions in Lu_2O_3, obtained using two methods (F-L and RM).

Considering the values of $\tau_{rad}(^4I_{11/2})$ of 4.96 ms and $B(^4I_{11/2} \rightarrow {}^4I_{15/2})$ of 0.833 obtained using the ICI model (see Table 4) for Er:Lu_2O_3, we achieve a $B(JJ')/\tau_{rad}$ of 169 s^{-1}, yielding a good agreement between the two approaches.

4. Luminescence lifetimes of $^4I_{11/2}$ and $^4I_{13/2}$ states of Er^{3+} ions

Prior to the lifetime studies, we measured the Raman spectra of Er:R_2O_3 crystals. For the cubic sesquioxide crystals under investigation, the set of irreducible representations for the optical modes at the center of the Brillouin zone Γ ($\boldsymbol{k}$ = 0) is $\Gamma_{op} = 4A_g + 4E_g + 14F_g + 5A_{2u} + 5E_u + 16F_u$, of which 22 modes ($A_g$, E_g and F_g) are Raman-active, 16 modes (F_u) are IR-active and the rest are silent [31]. The dominant Raman peak seen in Fig. 4 is assigned to $A_g + F_g$ vibrations. Its peak energy depends on the cation in the sesquioxide matrix. While it is found at 377 cm^{-1} in Er:Y_2O_3 its value increases to 390 cm^{-1} in Er:Lu_2O_3 and 416 cm^{-1} in Er:Sc_2O_3. The maximum phonon energy follows a similar trend: 593 cm^{-1} (Er:Y_2O_3), 611 cm^{-1} (Er:Lu_2O_3) and 666 cm^{-1} (Er:Sc_2O_3). These values are in good agreement with the values reported for undoped cubic rare-earth sesquioxide crystals [31].

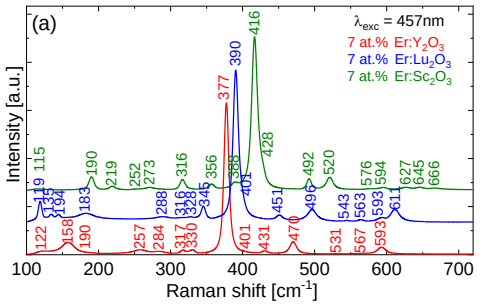

Fig. 4. Room-temperature unpolarized Raman spectra of 7 at.% Er^{3+}-doped sesquioxides, *numbers* – Raman peak energies in cm^{-1}, λ_{exc} = 457 nm.

The room-temperature (RT) luminescence lifetimes τ_{lum} of the $^4I_{11/2}$ and $^4I_{13/2}$ Er^{3+} states in yttria, scandia and lutetia for two reference doping levels (1 at.% and 7 at.% Er^{3+}) are compared in Fig. 5. The values presented here were measured under resonant excitation using finely powdered ceramic samples to avoid the effect of reabsorption. For both considered multiplets, the luminescence lifetime values tend to increase from Er:Sc_2O_3 to Er:Lu_2O_3 and further to Er:Y_2O_3, and this trend is more evident for the $^4I_{11/2}$ level. Considering the difference in the phonon spectra of sesquioxides as depicted in Fig. 4, as well as the relatively similar radiative transition probabilities as derived by the J-O theory for these compounds, this variation is assigned to the effect of non-radiative multiphonon relaxation. Increasing the Er^{3+} doping level from 1 at.% to 7 at.%, the $^4I_{13/2}$ luminescence lifetime is reduced while the $^4I_{11/2}$ lifetime remains almost unchanged. This is attributed to the previously mentioned concentration dependent

energy-transfer upconversion (ETU) process $^4I_{13/2} + {}^4I_{13/2} \rightarrow {}^4I_{15/2} + {}^4I_{11/2}$. The resulting improved ratio of the nearly constant $^4I_{11/2}$ lifetime and the quenched $^4I_{13/2}$ is favorable for 2.85 µm lasers based on the transition between these multiplets.

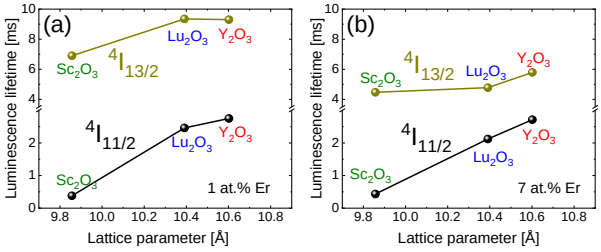

Fig. 5. Room temperature luminescence lifetimes of the $^4I_{11/2}$ and $^4I_{13/2}$ multiplets of (a) 1 at.% and (b) 7 at.% Er^{3+}-doped sesquioxides. The solid lines are guides to the eye with no physical meaning.

To explain the obvious difference between the luminescence and the radiative lifetimes of the $^4I_{11/2}$ and $^4I_{13/2}$ Er^{3+} states in sesquioxides, we studied the luminescence dynamics at different temperatures from room temperature down to 10 K. To minimize the influence of reabsorption and concentration quenching, we used samples with the lowest available Er^{3+} doping levels, *i.e.*, 0.3 at.% Er:Y_2O_3, 1.0 at.% Er:Lu_2O_3 and 0.3 at.% Er:Sc_2O_3.

First, we focused on the $^4I_{11/2}$ luminescence lifetimes. There are two emission channels from this state, the purely ED transition around 1 µm corresponding to the transition $^4I_{11/2} \rightarrow {}^4I_{15/2}$ and the 2.85 µm transition $^4I_{11/2} \rightarrow {}^4I_{13/2}$, which is ED and MD allowed with a strong MD component (see Table 3 and Table 4). Still, owing to the low luminescence branching ratio of the latter transition, the total MD contribution to the $^4I_{11/2}$ luminescence is very low. Thus, by looking at the $^4I_{11/2} \rightarrow {}^4I_{15/2}$ emission, we observe nearly exclusively the contribution of Er^{3+} ions on C_2 sites. Consequently, the luminescence decay curves measured under resonant excitation have a nearly single-exponential nature at 10 K and RT, as shown in Fig. 6(a,b). Note the significant difference of the corresponding luminescence lifetimes between the different host materials attributed to the different rates of non-radiative multiphonon relaxation (see above). This behavior is preserved even at 10 K.

The temperature dependence of the $^4I_{11/2}$ luminescence lifetimes τ_{lum} for low-doped sesquioxides shown in Fig. 6 (c) shows a maximum reached at different temperatures, depending on the host matrix. For Er:Y_2O_3 featuring the lowest phonon energies, the luminescence lifetime increases from 2.58 ms at RT to 4.25 ms at 10 K with a maximum at 25 K. The 10-K value is approaching the corresponding RT radiative lifetime of 5.39 ms (cf. Table 4). For Er:Lu_2O_3 and Er:Sc_2O_3, the longest lifetimes of 2.64 ms and 0.53 ms achieved at 50 K and 10 K, respectively remain well below the radiative lifetimes of around 5 ms in Table 4, indicating significant non-radiative decay even at 10 K.

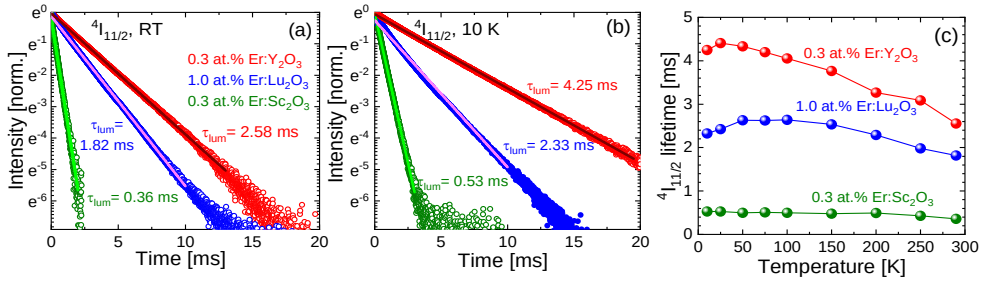

Fig. 6. (a,b) Luminescence decay curves of the $^4I_{11/2}$ multiplet of Er^{3+}-doped sesquioxides (a) at RT (290 K) and (b) 10 K, λ_{exc} = 960 nm, λ_{lum} = 1015 nm; the solid lines represent single exponential fits. (c) Temperature dependence of the luminescence lifetimes.

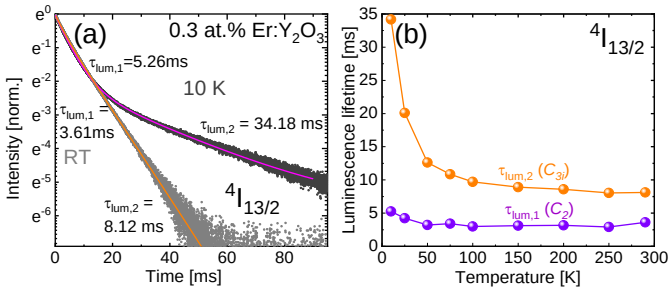

Fig. 7. Luminescence dynamics from the $^4I_{13/2}$ state of Er^{3+} ions in 0.3 at.% Er:Y_2O_3: (a) luminescence decay curves at RT and 10 K, the solid lines represent biexponential fits to the data, λ_{exc} = 1461 nm, λ_{lum} = 1543 nm; (b) temperature dependence of the 'fast' and 'slow' component of the biexponential fit.

For luminescence starting from the lowest excited multiplet $^4I_{13/2}$, the only emission channel is $^4I_{13/2} \rightarrow {}^4I_{15/2}$. The corresponding transition is ED and MD allowed with a strong MD contribution as seen in see Table 3. Thus, Er^{3+} ions on both sites, C_2 and C_{3i} contribute to the corresponding emission at 1.55 µm. With this in mind, we selected the excitation and emission wavelengths for the temperature dependent lifetime experiments to cover absorption and emission lines of Er^{3+} ions on C_2 and C_{3i} sites according to the crystal-field data given in [32] and applied a biexponential fit to the decay curves of this manifold, as shown in Fig. 7. As seen in Fig. 7 (a), the RT decay curve is hardly recognized as biexponential due to energy migration between the two sites at RT. In fact a biexponential fit would not yield reasonable results for the other two materials. Therefore, the values stated in Tab. 5 for the RT fluorescence lifetimes of the $^4I_{13/2}$ multiplet are based on single-exponential fits and thus averaged over both sites. Consequently, the corresponding decay curves were single exponential and are not shown here for brevity.

ED transitions are forbidden for ions on C_{3i} sites. The corresponding radiative lifetime was thus calculated accounting only for the MD component of the transition probability. The corresponding radiative lifetime $\tau_{rad} = 1/A(JJ')^{MD}$ is shown in the last column of Table 4. Consequently, different radiative lifetimes for ions on C_2 sites exhibiting both ED and MD contributions and ions on C_{3i} sites exhibiting pure MD transitions, are achieved. As expected, these values differ significantly; for Er:Y_2O_3, they amount to 5.79 ms and 13.2 ms, respectively. Consequently, the short and long component of the bi-exponential fits of the decay curves from the $^4I_{13/2}$ state can be assigned to Er^{3+} ions on C_2 and C_{3i} sites, respectively. For the case of 0.3 at.% Er:Y_2O_3 shown in Fig. 7(a,b) at RT, the fit yields 3.61 ms for the C_2 sites and 8.12 ms for the C_{3i} sites, while at 10 K values of 5.26 ms for C_2 sites and 34.18 ms for C_{3i} sites are obtained. It should be noted that the low temperature lifetime is mainly determined by transitions from the lower-lying Stark sub-levels of the $^4I_{13/2}$ multiplet, which can significantly differ from the radiative lifetime [33]. The value of 34 ms for the C_{3i} site is thus not in contradiction to the value of 13 ms listed in Tab. 4.

Table 5 summarizes the luminescence and radiative lifetimes of the $^4I_{11/2}$ and $^4I_{13/2}$ multiplets of Er^{3+} in low-doped sesquioxides. Our analysis reveals that the significant difference between the measured luminescence lifetime and the radiative lifetime derived from the absorption spectra originates from the presence of Er^{3+} ions on C_2 and C_{3i} sites, both significantly contributing to the ED and MD allowed $^4I_{13/2} \rightarrow {}^4I_{15/2}$ emission. Note that the Judd-Ofelt analysis for Er^{3+} has a low sensitivity to the contribution of ions on C_{3i} sites, because most of the considered transitions in absorption are MD forbidden and not influenced by ions on C_{3i} sites. Thus, assuming ¾ of the Er^{3+} ions being on C_2 sites and ¼ on C_{3i} sites allows to calculate the 'effective' transition probability as $\langle A \rangle = \frac{3}{4}A_{ED+MD}(C_2) + \frac{1}{4}A_{MD}(C_{3i})$, and the corresponding 'effective' radiative lifetime to be $\langle \tau_{rad} \rangle = 1/\langle A \rangle$. The resulting values are shown in Table 5 and are in good agreement with the measured room temperature luminescence lifetimes $\langle \tau_{lum} \rangle$.

Table 5. Luminescence and radiative lifetimes of the $^4I_{11/2}$ and $^4I_{13/2}$ Er^{3+} energy levels in sesquioxides

T	$^{2S+1}L_J$	Method	Lifetime, ms		
			Er:Y_2O_3	Er:Lu_2O_3	Er:Sc_2O_3
RT	$^4I_{11/2}$	τ_{lum}	2.58	1.82	0.36
		τ_{rad}, J-O	5.39	4.96	5.57
	$^4I_{13/2}$	$<\tau_{lum}>$	7.08	7.07	6.27
		τ_{rad}, J-O (C_2)	5.79	5.74	5.64
		τ_{rad}(MD), J-O (C_{3i})	13.22	13.86	14.73
		$<\tau_{rad}>$, J-O (¾:¼)	6.73	6.72	6.67
10 K	$^4I_{11/2}$	τ_{lum}	4.25	2.33	0.53
	$^4I_{13/2}$	$\tau_{lum,1}$ (C_2)	5.26	-	-
		$\tau_{lum,2}$ (C_{3i})	34.18	-	-

We thus conclude, that despite the presence of two different sites for Er^{3+} ions in cubic sesquioxides, the radiative lifetime of the $^4I_{11/2}$ state calculated via the Judd-Ofelt theory can be taken as a reliable value for further calculations of the effective stimulated-emission cross-sections. This is because most of the relevant transitions in Er^{3+} ions are forbidden for ions on C_{3i} sites and the C_2 sites considered by the J-O-theory mainly contribute also to emission from the $^4I_{11/2}$ multiplet. As for the $^4I_{13/2}$ level, we suggest that the 'effective' radiative lifetime $<\tau_{rad}>$ accounting for Er^{3+} ions located in both the C_2 and C_{3i} sites should be taken for calculating the stimulated-emission cross-sections at room temperature, where a strong energy exchange between the two ion ensembles prohibits the presence of emission from only one class of ions.

It is worth to note that at low temperatures the decay characteristics may strongly depend on the chosen excitation and detection wavelength. For Er^{3+} ions in Lu_2O_3 and Sc_2O_3, no information about the Stark level energies for C_{3i} sites is available. Thus, we were not yet successful in obtaining a full analysis of the temperature dependent luminescence dynamics starting from the $^4I_{13/2}$ multiplet for these materials.

5. Stimulated emission cross-sections

The $^4I_{13/2} \rightarrow {}^4I_{15/2}$ transition terminates at the ground state and as a consequence the corresponding emission at 1.55 µm is subject to reabsorption. Thus, for the calculation of the stimulated-emission cross-sections, we used two complementary methods: the reciprocity method (Eq. 8) [18] based on the $^4I_{15/2} \rightarrow {}^4I_{13/2}$ absorption cross-sections shown in Fig. 2(h), and the experimental crystal-field splitting of Er^{3+} ions on C_2 sites, and the F-L equation (Eq. 9) [34] based on the measured luminescence spectra. Using the effective luminescence lifetime $<\tau_{rad}>$ stated in Table 5 in the F-L equation, we get an excellent agreement of both methods. The results are shown in Fig. 8(a) for the three studied Er^{3+}-doped sesquioxide crystals. The stimulated-emission cross-sections in the long wavelength spectral range, where laser operation is expected due to the quasi-three-level laser scheme with reabsorption, peak at 1.61×10^{-21} cm^2 at 1641 nm for Er:Y_2O_3, 1.60×10^{-21} cm^2 at 1647 nm for Er:Lu_2O_3, and 1.58×10^{-21} cm^2 at 1667 nm for Er:Sc_2O_3.

For the $^4I_{11/2} \rightarrow {}^4I_{13/2}$ transition at 2.85 µm, only the F-L formula was applied using the τ_{rad} and B(JJ') values obtained from the J-O analysis. In the range of expected laser wavelengths, we found stimulated-emission cross-sections of 5.36×10^{-21} cm^2 at 2842 nm for Er:Y_2O_3, 5.67×10^{-21} cm^2 at 2845 nm Er:Lu_2O_3, and 3.57×10^{-21} cm^2 at 2857 nm for Er:Sc_2O_3. The emission of Er:Sc_2O_3 covers a wider wavelength range than those of Er^{3+} ions in Lu_2O_3 and Y_2O_3, due to a stronger crystal field which is resulting in a larger Stark splitting of the manifolds. This allows for lasing on longer wavelengths in comparison to materials with lower crystal field strengths.

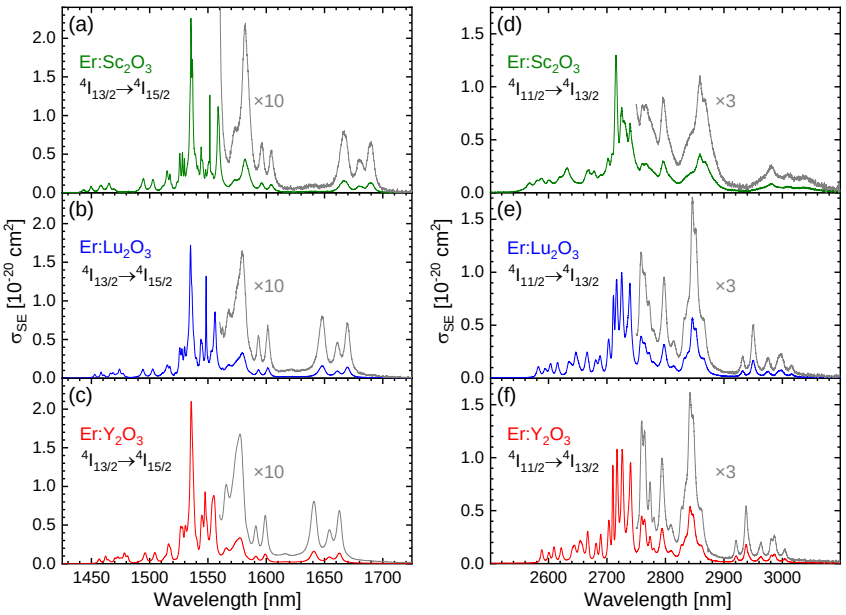

Fig. 8. Stimulated-emission (SE) cross-sections, σ_{SE}, for Er^{3+} ion in sesquioxide crystals: (a-c) the $^4I_{13/2} \rightarrow {}^4I_{15/2}$ transition; (d-f) the $^4I_{11/2} \rightarrow {}^4I_{13/2}$ transition.

6. Conclusion

In this work, we revisited the spectroscopic properties of three Er^{3+}-doped cubic sesquioxides, Y_2O_3, Lu_2O_3, and Sc_2O_3. The transition probabilities for Er^{3+} ions were calculated using the Judd-Ofelt theory accounting for the intermediate configuration interaction (ICI) based on the measured absorption cross-sections. To justify the obtained data on the radiative lifetimes of the $^4I_{11/2}$ and $^4I_{13/2}$ Er^{3+} states, we performed a detailed study of luminescence dynamics from these manifolds at different temperatures.

For the $^4I_{11/2}$ state, the luminescence lifetime both at RT and even at 10 K strongly depends on the host-forming cation in the sesquioxide matrix owing to a different rate of non-radiative multiphonon relaxation associated to a difference in the phonon spectra of sesquioxides. Y_2O_3 features the lowest phonon energies leading to the longest $^4I_{11/2}$ luminescence lifetime. The radiative lifetime of this level obtained via the Judd-Ofelt theory is assigned to Er^{3+} ions on C_2 sites. Consequently, the radiative lifetimes and branching ratios calculated by the J-O-theory enabled to calculate reliable emission cross sections in the wavelength range of 2.85 μm for the first time for Er:Y_2O_3, Er:Lu_2O_3 and Er:Sc_2O_3.

For the $^4I_{13/2}$ state, the transitions in absorption and emission are both ED and MD allowed and thus Er^{3+} ions residing on both C_2 and C_{3i} sites contribute to these processes. This is indeed confirmed in the present work by observing a biexponential decay from the $^4I_{13/2}$ manifold at different temperatures. The fast and slow time components of this decay are assigned to ions in C_2 and C_{3i} sites, respectively. The calculation of the radiative lifetime of the $^4I_{13/2}$ manifold by the Judd-Ofelt theory based on the measured absorption spectra yields a value being much shorter than the measured intrinsic luminescence lifetime at RT for samples doped with 1 at.% Er^{3+} or less. It is also shorter than the estimated radiative lifetime achieved from the comparison of the stimulated-emission cross-sections calculated by two different methods (F-L and RM). This difference is resolved by considering the contributions of Er^{3+} ions on C_2 and C_{3i} sites, *i.e.*, by calculating an 'effective' average radiative lifetime weighted by the occurrence of these sites. The use of this 'effective' radiative lifetime enabled to calculate stimulated-emission cross-sections for the $^4I_{13/2} \rightarrow {}^4I_{15/2}$ transition by the Füchtbauer-Ladenburg method, which are

in excellent agreement with those obtained from the absorption spectra by the reciprocity method.

The results obtained in this work will be of high relevance for the design, operation and further power scaling of 2.85-μm lasers based on Er^{3+}-doped sesquioxide gain materials.

Appendix A. Sample preparation and experimental methods

Synthesis of samples

The single-crystals of Er^{3+}-doped sesquioxides R_2O_3 (R = Y, Lu, Sc) used in the experiments performed for this work were grown by the heat exchanger method (HEM) employing rhenium (Re) crucibles in a closed setup. The starting materials (rare-earth oxides, 5N purity) were thoroughly mixed and filled into a crucible on top of a seed crystal placed in the Re crucible's appendix. The inductively heated crucible was kept in an isothermal insulation setup. The required temperature gradient for directed crystallization was ensured by a controlled flow of the cooling gas from the bottom of the crucible. By slowly reducing the heating power, the whole melt crystallized successively. More details can be found in [35].

For the absorption measurements, we used three Er^{3+}-doped single-crystals, Y_2O_3, Lu_2O_3 and Sc_2O_3. The actual Er^{3+} doping levels were determined by the X-ray fluorescence (XRF) method using a Bruker M4 Tornado spectrometer, to be 15.9 at.% Er:Y_2O_3, 12.5 at.% Er:Lu_2O_3 and 3.5 at.% Er:Sc_2O_3. The corresponding Er^{3+} ion densities N_{Er} were 0.427×10^{22} cm^{-3}, 0.428×10^{22} cm^{-3} and 0.117×10^{22} cm^{-3}, respectively.

In addition, for luminescence lifetime studies, we used two low-doped crystals, 0.3 at.% Er:Y_2O_3 and 0.3 at.% Er:Sc_2O_3 and a 1 at.% Er:Lu_2O_3 ceramic sample.

For measuring the concentration-dependent luminescence lifetimes of Er^{3+} ions, we used a set of transparent sesquioxide ceramics with 1 at.% and 7 at.% Er^{3+} doping. The ceramics were prepared by hot pressing of nanopowders. Commercial rare-earth oxide powders (4N purity) were dissolved in nitric acid (6N) and mixed in the given ratios. We added glycine (3N) in a molar ratio of 1:1 with respect to the nitrate groups and 1 wt.% of LiF (3N) with respect to the oxide powder acting as a sintering aid. The precursors were placed in a furnace preheated to 500 °C, resulting in the synthesis of Er^{3+}-doped sesquioxide nanopowders. These were placed in a graphite mold and hot pressed under 50 MPa at a temperature of 1500 °C for Er:Y_2O_3 or 1600 °C for Er:Sc_2O_3 and Er:Lu_2O_3 for 1 h under a vacuum of about 10 Pa. The ceramics were then annealed in air at 900 °C for 5 h.

Experimental methods

The room temperature (RT, 290 K) transmission spectra of Er^{3+}-doped sesquioxide crystals were measured in the wavelength range between 270 and 1700 nm using a Perkin Elmer Lambda 1050 spectrometer. The spectral bandwidth (SBW) was 0.04 – 0.1 nm, depending on the spectral range and required resolution. The absorption cross-sections were calculated as $\sigma_{abs} = \alpha_{abs}/N_{Er}$, where α_{abs} is the absorption coefficient calculated via the Beer-Lambert law.

The RT Raman spectra were measured using a Renishaw InVia confocal laser microscope equipped with an Ar^+ ion laser (458 nm) and a 50× Leica objective.

The luminescence dynamics were studied by employing an optical parametric oscillator (GWU versaScan) pumped by a frequency tripled 10-Hz, 5-ns Nd^{3+}-laser (Spectra-Physics Quanta-Ray) as the excitation source, a 1 m monochromator (Horiba 1000M Series II) and a near-infrared photomultiplier module (Hamamatsu NIR-PMT H10330A-75) as well as a 2 GHz digital oscilloscope (Rohde&Schwarz RTE 1204). For low-temperature studies, the samples were mounted in a closed-cycle helium cryostat (Advanced Research Systems DE-204P).

The luminescence spectra were measured using a cw Ti:sapphire laser (3900S, Spectra Physics) as an excitation source and optical spectrum analyzers (Yokogawa AQ6376 and AQ6375B) using a ZrF_4 fiber for light collection.

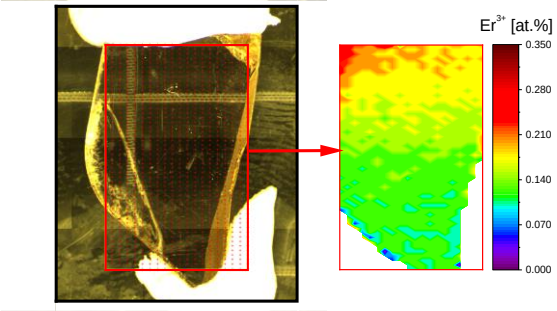

Fig. A1. Spatial distribution of dopant Er^{3+} ions across a 0.3 at.% Er:Sc_2O_3 crystal (doping level in the melt) determined by XRF analysis: the left image shows a photography of the sample; the grid shows the points on which the high resolution compositional analysis was performed and the red rectangle marks the full analyzed area of 8.37 × 12.87 mm^2; the right side shows the results of the Er^{3+} element mapping.

For Er:Y_2O_3 and Er:Lu_2O_3 crystals, the gradient of Er^{3+} doping across the studied samples was found to be low and the segregation coefficient $K_{Er} = C_{crystal}/C_{melt}$ was close to unity. In contrast, for Sc_2O_3, we observed a strong gradient of the dopant ion concentration, which is explained by the large difference of the ionic radii of Er^{3+} (0.89 Å) and Sc^{3+} (0.75 Å) [36] in the sixfold oxygen coordination. Figure A1 shows a photograph of a 0.3 at.% Er:Sc_2O_3 sample (doping level in the melt) used for the low temperature luminescence lifetime studies and the corresponding spatial distribution of the Er^{3+} doping ions determined by XRF. The bottom part of the sample shown in this figure corresponds to the beginning of crystallization during the crystal growth and its upper part to the end of the crystal growth. A strong gradient of the actual Er^{3+} doping level from less than 0.1 at.% in the bottom part up to 0.35 at.% in the upper part is observed. By fitting these data with the Scheil equation [37], we estimated the segregation coefficient K_{Er} of about 0.35 in good agreement with the previous data [38]. A similar analysis was performed for the Er:Sc_2O_3 sample used for absorption studies resulting in a nearly identical K_{Er} value. For calculating the absorption cross-sections for Er^{3+} ions in Sc_2O_3, the average Er^{3+} doping level in the region of the transmitted light beam was then used.

Acknowledgment. We acknowledge the help of Stefan Püschel in determining the XRF-measurements.

Funding. French Agence Nationale de la Recherche (ANR) SPLENDID2 (ANR-19-CE08-0028). “RELANCE” Chair of Excellence project funded by the Normandy Region. Russian Science Foundation (research project No. 21-13-00397).

Disclosures. The authors declare no conflicts of interest.

Data availability. Data underlying the results presented in this paper are not publicly available at this time but may be obtained from the authors upon reasonable request.

References

1. V.A. Serebryakov, É.V. Boĭko, N.N. Petrishchev, and A.V. Yan, "Medical applications of mid-IR lasers. Problems and prospects," J. Opt. Technol. **77** (1), 6-17 (2010).
2. U. Elu, L. Maidment, L. Vamos, F. Tani, D. Novoa, M.H. Frosz, V. Badikov, D. Dadikov, V. Petrov, P.S.J. Russell, and J. Beigert, "Seven-octave high-brightness and carrier-envelope-phase-stable light source," Nat. Photonics **15** (4), 277-280 (2021).
3. J. Haas and B. Mizaikoff, "Advances in Mid-Infrared Spectroscopy for Chemical Analysis," Annu. Rev. Anal. Chem. **9** (1), 45-68 (2016).
4. C. Kränkel, "Rare-earth-doped sesquioxides for diode-pumped high-power lasers in the 1-, 2-, and 3-µm spectral range," IEEE J. Sel. Top. Quant. Electron. **21** (1), 1602013 (2015).
5. P.A. Loiko, K.V. Yumashev, R. Schödel, M. Peltz, C. Liebald, X. Mateos, B. Deppe, and C. Kränkel, "Thermo-optic properties of Yb:Lu_2O_3 single crystals," Appl. Phys. B **120** (4), 601-607 (2015).
6. L. Laversenne, Y. Guyot, C. Goutaudier, M.T. Cohen-Adad, and G. Boulon, "Optimization of spectroscopic properties of Yb^{3+}-doped refractory sesquioxides: Cubic Y_2O_3, Lu_2O_3 and monoclinic Gd_2O_3," Opt. Mater. **16**, 475-483 (2001).

7. M.J. Weber, "Radiative and Multiphonon Relaxation of Rare-Earth Ions in Y_2O_3," Phys. Rev. **171** (2), 283-291 (1968).
8. M. Pollnau, W. Lüthy, and H.P. Weber, "Explanation of the cw operation of the Er^{3+} 3-μm crystal laser," Phys. Rev. A **49** (6), 3990-3996 (1994).
9. W. Yao, H. Uehara, S. Tokita, H. Chen, D. Konishi, M. Murakami, and R. Yasuhara, "LD-pumped 2.8 μm Er:Lu2O3 ceramic laser with 6.7 W output power and >30% slope efficiency," Appl. Phys. Express **14** (1), 012001 (2021).
10. L. Wang, H.T. Huang, D.Y. Shen, J. Zhang, H. Chen, and D.Y. Tang, "Diode-pumped high power 2.7μm Er:Y_2O_3 ceramic laser at room temperature," Opt. Mat. **71**, 70-73 (2017).
11. T. Li, K. Beil, C. Kränkel, and G. Huber, "Efficient high-power continuous wave Er:Lu_2O_3 laser at 2.85 μm," Opt. Lett. **37** (13), 2568-2570 (2012).
12. M.M. Ding, X.X. Li, F. Wang, D.Y. Shen, J. Wang, D.Y. Tang, and H.Y. Zhou, "Power scaling of diode-pumped Er:Y_2O_3 ceramic laser at 2.7 μm," Appl. Phys. Express **15** (062004), (2022).
13. Z.D. Fleischman and T. Sanamyan, "Spectroscopic analysis of Er^{3+}:Y_2O_3 relevant to 2.7 μm mid-IR laser," Opt. Mat. Express **6** (10), 3109-3118 (2016).
14. W.T. Carnall, P.R. Fields, and K. Rajnak, "Electronic Energy Levels in the Trivalent Lanthanide Aquo Ions. I. Pr^{3+}, Nd^{3+}, Pm^{3+}, Sm^{3+}, Dy^{3+}, Ho^{3+}, Er^{3+}, and Tm^{3+}," J. Chem. Phys. **49** (10), 4424-4442 (1968).
15. R. Ladenburg, "Die quantentheoretische Deutung der Zahl der Dispersionselektronen," Z. Phys. **4** (4), 451-468 (1921).
16. B.R. Judd, "Optical Absorption Intensities of Rare-Earth Ions," Phys. Rev. **127** (3), 750-761 (1962).
17. G.S. Ofelt, "Intensities of Crystal Spectra of Rare - Earth Ions," J. Chem. Phys. **37**, 511-520 (1962).
18. D.E. McCumber, "Einstein relations connecting broadband emission and absorption spectra," Phys. Rev. **136** (4A), 954-957 (1964).
19. S.A. Payne, L.L. Chase, L.K. Smith, W.L. Kway, and W.F. Krupke, "Infrared cross-section measurements for crystals doped with Er^{3+}, Tm^{3+}, and Ho^{3+}," IEEE J. Quantum Elect. **28** (11), 2619 (1992).
20. M.J. Kobrinsky, B.A. Block, J.-F. Zheng, B.C. Barnett, E. Mohammed, M. Reshotko, F. Robertson, S. List, I. Young, and K. Cadien, "On-Chip Optical Interconnects," Intel Technol. J. **8** (02), 129-141 (2004).
21. L.D. Merkle, N. Ter-Gabrielyan, N.J. Kacik, T. Sanamyan, H.J. Zhang, H.H. Yu, J.Y. Wang, and M. Dubinskii, "Er:Lu_2O_3 - Laser-related spectroscopy," Opt. Mat. Express **3** (11), 1992-2002 (2013).
22. C.R. Stanek, K.J. McClellan, B.P. Uberuaga, K.E. Sickafus, M.R. Levy, and R.W. Grimes, "Determining the site preference of trivalent dopants in bixbyite sesquioxides by atomic-scale simulations," Phys. Rev. B **75**, 134101 (2007).
23. D.E. Zelmon, J.M. Northridge, N.D. Haynes, D. Perlov, and K. Petermann, "Temperature-dependent Sellmeier equations for rare-earth sesquioxides," Appl. Opt. **52** (16), 3824-3828 (2013).
24. P. Loiko, A. Volokitina, X. Mateos, E. Dunina, A. Kornienko, E. Vilejshikova, M. Aguilo, and F. Diaz, "Spectroscopy of Tb^{3+} ions in monoclinic $KLu(WO_4)_2$ crystal application of an intermediate configuration interaction theory," Opt. Mater. **78**, 495-501 (2018).
25. A.A. Kornienko, A.A. Kaminskii, and E.B. Dunina, "Dependence of the Line Strength of f–f Transitions on the Manifold Energy. II. Analysis of Pr^{3+} in $KPrP_4O_{12}$," Phys. Stat. Sol. (b) **157** (1), 267-273 (1990).
26. Y.Y. Yeung and P.A. Tanner, "Trends in Atomic Parameters for Crystals and Free Ions across the Lanthanide Series: The Case of $LaCl_3$:Ln^{3+}," J. Phys. Chem. A **119** (24), 6309-6316 (2015).
27. V. Peters, Growth and Spectroscopy of Ytterbium-Doped Sesquioxides, Book, Hamburg, (2001).
28. C. Kränkel, D. Fagundes-Peters, S.T. Fredrich, J. Johannsen, M. Mond, G. Huber, M. Bernhagen, and R. Uecker, "Continuous wave laser operation of Yb^{3+}:YVO_4," Appl. Phys. B **79**, 543-546 (2004).
29. H. Kühn, S.T. Fredrich-Thornton, C. Kränkel, R. Peters, and K. Petermann, "Model for the calculation of radiation trapping and description of the pinhole method," Opt. Lett. **32** (13), 1908-1910 (2007).
30. H. Kühn, K. Petermann, and G. Huber, "Correction of reabsorption artifacts in fluorescence spectra by the pinhole method," Opt. Lett. **35** (10), 1524-1526 (2010).
31. M.V. Abrashev, N.D. Todorov, and J. Geshev, "Raman spectra of R_2O_3 (R—rare earth) sesquioxides with C-type bixbyite crystal structure: A comparative study," J. Appl. Phys. **116** (10), 103508 (2014).
32. J.B. Gruber, R.P. Leavitt, C.A. Morrison, and N.C. Chang, "Optical spectra, energy levels, and crystal-field analysis of tripositive rare-earth ions in Y_2O_3. IV. C_{3i} sites," J. Chem. Phys. **82** (12), 5373-5377 (1985).
33. S. Püschel, S. Kalusniak, C. Kränkel, and H. Tanaka, "Temperature-dependent radiative lifetime of Yb:YLF: refined cross sections and potential for laser cooling," Opt. Express **29** (7), 11106-11120 (2021).
34. C. Füchtbauer, G. Joos, and O. Dinkelacker, "Über Intensität, Verbreiterung und Druckverschiebung vor Spektrallinien, insbesondere der Absorptionslinie 2537 des Quecksilbers," Ann. Phys. **376** (9-12), 204-227 (1923).
35. R. Peters, C. Kränkel, K. Petermann, and G. Huber, "Crystal growth by the heat exchanger method, spectroscopic characterization and laser operation of high-purity Yb:Lu_2O_3," J. Cryst. Growth **310** (7-9), 1934-1938 (2008).
36. A.A. Kaminskii, "Laser crystals - their physics and properties", Second Edition ed., Springer-Verlag, Heidelberg (1990).
37. E. Scheil, "Bemerkungen zur Schichtkristallbildung," Z. Metallk. **34** (3), 70-72 (1942).
38. A. Heuer, "Rare-earth-doped sesquioxides for lasers in the mid-infrared spectral range," Department of Physics, Universität Hamburg, (2018).